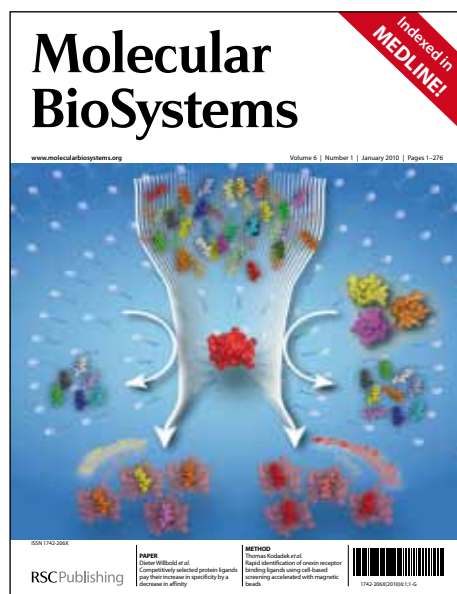


# Molecular Biosystems

Accepted Manuscript



This is an *Accepted Manuscript*, which has been through the RSC Publishing peer review process and has been accepted for publication.

*Accepted Manuscripts* are published online shortly after acceptance, which is prior to technical editing, formatting and proof reading. This free service from RSC Publishing allows authors to make their results available to the community, in citable form, before publication of the edited article. This *Accepted Manuscript* will be replaced by the edited and formatted *Advance Article* as soon as this is available.

To cite this manuscript please use its permanent Digital Object Identifier (DOI®), which is identical for all formats of publication.

More information about *Accepted Manuscripts* can be found in the [Information for Authors](#).

Please note that technical editing may introduce minor changes to the text and/or graphics contained in the manuscript submitted by the author(s) which may alter content, and that the standard [Terms & Conditions](#) and the [ethical guidelines](#) that apply to the journal are still applicable. In no event shall the RSC be held responsible for any errors or omissions in these *Accepted Manuscript* manuscripts or any consequences arising from the use of any information contained in them.

# Kinetic mechanism of human thymidine phosphorylase – a molecular target for cancer drug development.

Candida Deves<sup>1,2</sup>, Diana Carolina Rostirolla<sup>1,2</sup>, Leonardo Kras Borges Martinelli<sup>1</sup>, Cristiano Valim Bizarro<sup>1</sup>, Diogenes Santiago Santos<sup>1,2\*</sup>, Luiz Augusto Basso<sup>1,2\*</sup>.

<sup>1</sup>Centro de Pesquisas em Biologia Molecular e Funcional (CPBMF), Instituto Nacional de Ciência e Tecnologia em Tuberculose (INCT-TB), Pontifícia Universidade Católica do Rio Grande do Sul (PUCRS), 6681/92-A Av. Ipiranga, 90619-900, Porto Alegre, RS, Brazil.

<sup>2</sup>Programa de Pós-Graduação em Medicina e Ciências da Saúde, Pontifícia Universidade Católica do Rio Grande do Sul (PUCRS), Porto Alegre, RS, Brazil.

\*Corresponding authors: Luiz A. Basso or Diógenes S. Santos

Av. Ipiranga 6681 – Tecnopuc – Prédio 92A, ZIP CODE 90619-900, Porto Alegre, RS, Brazil. Phone/Fax: +55-51-33203629; E-mail addresses: [luiz.basso@pucrs.br](mailto:luiz.basso@pucrs.br) or [diogenes@pucrs.br](mailto:diogenes@pucrs.br)

Running title: Kinetic mechanism of human thymidine phosphorylase.

## Summary

Human thymidine phosphorylase (HTP), also known as platelet-derived endothelial cell growth factor (PD-ECGF) or gliostatin, catalyzes the reversible phosphorolysis of thymidine (dThd) to thymine and 2-deoxy- $\alpha$ -D-ribose-1-phosphate (2dR1P). HTP is a key enzyme in the pyrimidine salvage pathway involved in dThd homeostasis in cells. HTP is a target for anticancer drug development as its enzymatic activity promotes angiogenesis. Here, we describe cloning, expression, and purification to homogeneity of recombinant *TYMP*-encoded HTP. Peptide fingerprinting and molecular mass value of the homogenous protein confirmed its identity as HTP assessed by mass spectrometry. Size exclusion chromatography showed that HTP is a dimer in solution. Kinetic studies revealed that HTP displayed substrate inhibition for dThd. Initial velocity and isothermal titration calorimetry (ITC) studies suggest that HTP catalysis follows a rapid-equilibrium random bi-bi kinetic mechanism. ITC measurements also showed that dThd and  $P_i$  binding are favorable processes. The pH-rate profiles indicated that maximal enzyme activity was achieved at low pH values. Functional groups with apparent  $pK$  values of 5.2 and 9.0 are involved in dThd binding and groups with  $pK$  values of 6.1 and 7.8 are involved in phosphate binding.

*Keywords:* Human thymidine phosphorylase; initial velocity; isothermal titration calorimetry; kinetic mechanism; pH-rate profile.

## Introduction

Human Thymidine Phosphorylase (HTP; EC 2.4.2.4) belongs to the pyrimidine nucleoside phosphorylase (PYNP) family,<sup>1</sup> and plays an important role in nucleotide metabolism<sup>2</sup>. In mammalian cells, there are two enzymes from this family: Thymidine Phosphorylase (TP) and Uridine Phosphorylase (UP), whereas in lower organisms there exists only one enzyme, Pyrimidine Nucleoside Phosphorylase (PyNP). PyNP accepts both thymidine and uridine as natural substrates. TP is highly specific for 2'-deoxynucleosides of thymine and related pyrimidine bases, whereas UP does not distinguish between ribose and deoxyribose in pyrimidine nucleosides.<sup>2</sup> HTP is also known as platelet-derived endothelial cell growth factor (PD-ECGF)<sup>3</sup> or gliostatin.<sup>4</sup> HTP, which is functionally active as a homodimer, is involved in the salvage pathway of pyrimidine nucleotides, ensuring that a sufficient pool of pyrimidine nucleotides is available for DNA repair and replication.<sup>5,6</sup> In the presence of inorganic phosphate, this enzyme catalyzes the reversible phosphorolysis of 2'-deoxythymidine (dThd) to thymine and 2-deoxy- $\alpha$ -D-ribose-1-phosphate (2dR1P) (Fig. 1), and its main metabolic function appears to be catabolic.<sup>7</sup> HTP has also a deoxyribosyl transferase activity by which the deoxyribosyl moiety is transferred from a pyrimidine nucleoside to another pyrimidine base, resulting in the formation of a new pyrimidine nucleoside.<sup>8</sup>

HTP plays an important role in the pathogenesis of cancer. The angiogenic activity of HTP plays a significant function in tumor biology, promoting new capillary blood vessel formation.<sup>9</sup> High levels of HTP expression in tumor cells have been correlated with poor prognoses.<sup>10</sup> HTP lacks a signal sequence indicating that HTP is not secreted from carcinoma cells and should thus act indirectly on the endothelial cells. HTP enzymatic activity is reported to be required for new capillary formation, as

mutagenesis of the enzyme's active-site residues abolish the angiogenic activity.<sup>11-13</sup> HTP is linked to angiogenesis by the production of 2-deoxyribose (2dR) from dThd, and this sugar is considered a chemoattractant that stimulates endothelial cell migration.<sup>14,15</sup> During catalysis, HTP releases the monosaccharide 2dR1P and its dephosphorylation within the cytoplasm permits extracellular release of the 2dR product.<sup>16</sup> 2dR is considered the main factor causing the angiogenic switch and the association between TP activity and angiogenesis is based on the potential accumulation of dThd-derived sugars from the HTP-catalyzed chemical reaction.<sup>15,17</sup>

Besides the natural 2'-deoxynucleoside thymidine and 2'-deoxyuridine, HTP recognizes and plays a role in the catabolic inactivation of several pyrimidines or pyrimidine nucleosides with antiviral and antitumoral activity, such as 5-(E)-(2-bromovinyl)-2'-deoxyuridine (BVDU), 5-trifluorothymidine (TFT), 5-iodo-2'-deoxyuridine (IDU), or 5-fluoro-2'-deoxyuridine (FDU). Therefore, administration of such therapeutic agents with an HTP inhibitor could improve the biological efficacy of these nucleoside analogues.<sup>18</sup> On the other hand, HTP has been involved in the activation of several prodrugs of the antitumour agent 5-Fluorouracil, such as tegafur (1-(tetrahydro-2-furanyl)-5-fluorouracil) and capecitabine (4-N-pentyloxycarbonyl-5'-deoxy-5-fluorocytidine). Under therapeutic regimens that include these prodrugs, HTP inhibitors would thus be incompatible.<sup>19,20</sup>

As HTP contributes significantly to angiogenesis, tumor progression and metastasis, studies are required to reveal the mode of action of HTP. Understanding the mode of action of HTP will inform us on how to better design inhibitors targeting this enzyme. These inhibitors may block HTP activity *in vivo* and, hopefully, suppress tumor growth and reduce metastasis.<sup>6,11,12,17,21</sup> To date, a number of inhibitors have been designed and tested for their efficacy in inhibiting HTP. Current inhibitors are mainly

substrate analogues, while some synthetic inhibitors and purine-based inhibitors have also been reported.<sup>9</sup> One of the most potent inhibitors, 5-chloro-6-[1-(2-iminopyrrolidinyl)methyl]uracil hydrochloride (TPI), caused a reduction in the rate of tumor growth when administrated to mice carrying tumors that overexpressed HTP.<sup>22</sup>

Efforts to develop new and potent HTP inhibitors have followed different strategies.<sup>23-25</sup> The structure of HTP co-crystalized with one of the most potent inhibitor TPI,<sup>26</sup> the molecular model of HTP in complex with "hits" derived from computational screening of the National Cancer Institute database,<sup>27</sup> the structure of the transition state of HTP determined from multiple kinetic isotope effect analysis and computer modeling,<sup>28,29</sup> provide different avenues for the rational design of selective inhibitors.

Here, we describe amplification, cloning and cDNA sequencing of the *TYMP* gene (NM\_001953.4) from colorectal tumour tissue. We also present heterologous protein expression in *E. coli*, purification to homogeneity, mass spectrometry, oligomeric state determination, substrate inhibition and pH-rate profiles. Additionally, the determination of true steady-state kinetics and isothermal titration calorimetry (ITC) measurements of substrate/product binding were performed to provide further evidence on HTP enzyme kinetic mechanism. The results described here should augment our knowledge on HTP mode of action and be useful to efforts to HTP-targeted development of inhibitors with potential anti-cancer activity.

## Results and discussion

### Amplification, cloning and DNA sequencing of the *TYMP* gene

The human *TYMP* gene region coding the mature HTP, P19971[11 – 482] was PCR amplified in the presence of 5% DMSO in the reaction mixture (data not shown). The addition of DMSO co-solvent in the mixture helps the denaturation of CG-rich DNAs,<sup>30</sup> which is consistent with a high G+C content of the *TYMP* gene<sup>31</sup>. The PCR product consistent with the expected size (1415 bp) was detected by agarose gel electrophoresis, purified, and cloned into the pCR-Blunt vector. Subsequently, the insert was subcloned into the pET-23a(+) expression vector and insertion of the DNA fragment confirmed by *NdeI* and *HindIII* enzyme restriction analysis. Nucleotide sequence of the cloned fragment corresponding to the human *TYMP* coding sequence was confirmed by automated DNA sequencing, revealing the integrity of the gene and absence of mutations that could have been introduced by the DNA amplification step.

### Expression and purification of recombinant HTP

The pET-23a(+):*TYMP* recombinant plasmid was transformed into Rosetta (DE3) *E. coli* cells by electroporation and culture was grown in TB medium for 48h. The cells were disrupted by sonication and the supernatant, following clarification by centrifugation, was analyzed for protein expression at different periods of cell growth after reaching an  $OD_{600nm} = 0.4 - 0.6$ . Sodium dodecyl sulfate-polyacrylamide gel electrophoresis (SDS-PAGE) analysis confirmed the expression of a protein in the soluble fraction with apparent subunit molecular mass of ~50 kDa, in agreement with the predicted molecular mass for HTP (49,024.3 Da). SDS-PAGE analysis also showed that the highest expression of soluble recombinant HTP was obtained at 24h in TB

medium at 37°C, without isopropyl- $\beta$ -D-thiogalactopyranoside (IPTG) induction (data not shown). In agreement with our result, high levels of protein expression in the absence of inducer have been shown to occur in the pET system.<sup>32,33</sup> In the pET vector system, target genes are positioned downstream of the strong bacteriophage T7 late promoter.<sup>34</sup> It has been proposed that leaky protein expression is due to a property of the *lac*-controlled system when cells approach stationary phase in complex medium and that cyclic adenosine monophosphate, acetate, and low pH are required to achieve high-level expression in the absence of IPTG induction, which may be part of the general cellular response to nutrition limitation.<sup>35</sup> However, it has later been shown that unintended induction in the pET system is due to the presence of as little as 0.0001% of lactose in the medium.<sup>36</sup>

The expressed recombinant HTP protein was purified to homogeneity (Fig. 2) by a two-step protocol consisting of an anion-exchange column (Q-Sepharose Fast Flow) and a hydrophobic interaction column (HiLoad Phenyl Sepharose High performance). The recombinant HTP eluted at approximately 150 mM of NaCl from the anion exchange column, and samples containing the target protein were dialyzed against buffer A to remove remaining salt. Homogeneous recombinant HTP was obtained from the hydrophobic interaction column elution at approximately 255 mM of ammonium sulfate, and again dialyzed against buffer A to desalt. This 18-fold purification protocol yielded 12 mg of homogeneous recombinant HTP from 7.6 g of wet cells indicating a protein yield of 52% (Table 1). Homogeneous enzyme was stored at – 80°C with no loss of activity.

**Table 1.** Purification of recombinant HTP expressed in *E. coli* Rosetta (DE3) cells.

Typical purification protocol from 7.6 g wet cell paste.

Purification Step	Total protein (mg)	Total enzyme activity <sup>a</sup> (U)	Specific activity (U mg <sup>-1</sup> )	Purification fold	Yield (%)
Crude extract	410	98	0.24	1.0	100
Q-Sepharose FF	25	47	1.91	8	48
Phenyl Sepharose	12	52	4.3	17.9	52

<sup>a</sup> One unit (U) of enzyme is the amount of HTP that converts 1  $\mu$ mol of dThd and P<sub>i</sub> to thymine and 2dR1P per minute at pH 7.5 at 37°C.

### Identification and determination of HTP molecular mass by Mass Spectrometry

In order to determine the HTP molecular mass, we performed intact protein analysis using an Orbitrap analyzer. The average spectra from 417 scans spanning charge states 29+ to 65+ was deconvoluted and we found a value of 48,855 Da for the average molecular mass of HTP (Fig. 3). However, the theoretical molecular mass for the mature HTP [11-482] with the N-terminal methionine removed is 49,024.3 Da, implying a difference of 168 Da between expected and experimentally found values. We hypothesized that recombinant mature HTP could have lost the first two residues (Ala11 and Pro12), which would result in a truncated protein of 48,856 Da, in good agreement with the experimentally observed molecular mass.

In order to test this hypothesis, we performed LC-MS/MS peptide mapping experiments. We compared the MS/MS spectra of HTP with the human proteome including the amino acid sequences from the mature [11-482] and the truncated version of HTP [13-482]. From 582 spectra, we identified 36 different peptides covering 80.98% of the truncated HTP primary sequence, including the N-terminal peptide PAPGDFSGEGSQGLPDPSPEPK found in 32 different spectra. This peptide starts at Pro13 and is supposed to be found only in the truncated [13-482] HTP form. Moreover, when compared to the mature HTP sequence [11-482], we did not detect the

corresponding N-terminal peptide APPAPGDFSGEGSQGLPDPSPEPK. These results are in agreement with our data from intact protein analysis experiments, indicating that the recombinant HTP starts at Pro13.

### **Determination of oligomeric state of HTP in solution**

The molecular mass of recombinant HTP was determined by size exclusion chromatography. The recombinant HTP eluted as a single peak at 12.47 mL, which corresponds to an apparent molecular mass value of 120,100 Da. Molecular mass value was divided by HTP subunit molecular mass (49,024.3 Da), and the value of 2.4 obtained indicates that HTP is likely a dimer in solution. This result is in agreement with the HTP structural analysis, in which the HTP is homodimeric.<sup>26,37,38</sup> In addition, crystal structure analysis revealed that *E. coli* TP<sup>39</sup> and Pyrimidine nucleoside phosphorylase (PYNP) from *Bacillus stearothermophilus*<sup>40</sup> are dimeric proteins which, structurally, do not differ from higher eukaryotes.

### **Determination of apparent steady-state kinetic constants and initial velocity patterns**

The determination of apparent steady-state kinetic constants was performed using either P<sub>1</sub> or dThd as the variable substrate. The dependence of initial velocity on increasing P<sub>1</sub> concentrations, at fixed-saturating dThd concentration (400 μM), followed hyperbolic Michaelis-Menten kinetics (Fig. 4A).<sup>41</sup> The apparent Michaelis-Menten constant ( $K_M$ ) and the catalytic constant ( $k_{cat}$ ) for P<sub>1</sub> were, respectively, 218 (± 15) μM and 8.7 (± 0.2) s<sup>-1</sup>. The dependence of velocity on increasing concentrations of dThd (Fig. 4B), at fixed-saturating P<sub>1</sub> concentration (2 mM), revealed substrate inhibition at high dThd levels, as there was a decrease in enzyme velocity at dThd concentration values larger than 500

$\mu\text{M}$ . The apparent steady-state parameters were:  $k_{\text{cat}} = 9.9 (\pm 0.2) \text{ s}^{-1}$ ,  $K_{\text{dThd}} = 130 (\pm 6) \mu\text{M}$ , and  $K_{\text{idThd}} = 895 (\pm 48) \mu\text{M}$ , which is approximately 7-fold larger than the  $K_{\text{dThd}}$  value. The  $k_{\text{cat}}$  value here determined is similar to the apparent steady kinetic constants previously reported by Schwartz *et al*<sup>29</sup> for HTP, while the  $K_{\text{dThd}}$  is larger than the value calculated from data fitting to Michaelis-Menten equation in the absence of substrate inhibition ( $30 \pm 4 \mu\text{M}$ ).<sup>29</sup> Additionally, the apparent  $K_{\text{M}}$  value for  $\text{P}_i$  is 20-fold larger than the one reported for HTP-catalyzed phosphorolytic depyrimidation of dThd ( $11 \pm 2 \mu\text{M}$ ).<sup>29</sup>

Initial velocity patterns were employed to determine the true Michaelis-Menten constants from primary double-reciprocal plots of the steady-state, and the kinetic mechanism for the forward reaction (phosphorolysis) catalyzed by HTP. The family of lines intersecting to the left of the  $y$ -axis (Fig. 5A and B) for both substrates are consistent with ternary complex formation and a sequential mechanism.<sup>41</sup> The data were fitted to Eq. (6), yielding the following true steady-state kinetic parameters:  $k_{\text{cat}} = 7.2 (\pm 0.2) \text{ s}^{-1}$ ,  $K_{\text{dThd}} = 66 (\pm 5) \mu\text{M}$  and  $K_{\text{Pi}} = 107 (\pm 7) \mu\text{M}$ . The calculated values for the specificity constants ( $k_{\text{cat}}/K_{\text{M}}$ ) for dThd and  $\text{P}_i$  are, respectively,  $1.09 (\pm 0.06) \times 10^5 \text{ M}^{-1} \text{ s}^{-1}$  and  $6.7 (\pm 0.3) \times 10^4 \text{ M}^{-1} \text{ s}^{-1}$ . As observed in Fig. 5A, substrate inhibition by dThd is apparently more pronounced at fixed and low concentration of  $\text{P}_i$  ( $70 \mu\text{M}$ ) and at high concentration of dThd. Nevertheless, in physiological environments this condition is not likely to occur, since the intracellular concentration of  $\text{P}_i$  is larger than  $4 \text{ mM}$ ,<sup>42</sup> exceeding its  $K_{\text{M}}$  value for HTP. A similar initial velocity pattern was observed for TP from mouse liver,<sup>43</sup> *Escherichia coli*<sup>44</sup>, *Salmonella typhimurium*<sup>45</sup>, *Lactobacillus casei*<sup>46</sup>, and for human UP.<sup>32</sup> The ping-pong and rapid equilibrium ordered enzyme mechanisms could be ruled out, since these mechanisms give double-reciprocal plots of, respectively, parallel lines and intersecting lines at the  $y$ -axis. The sequential

mechanism indicates that enzymatic catalysis only occurs when both substrates are bound to the enzyme active site. It has been pointed out that the occurrence of substrate inhibition can be observed for ping-pong and steady-state ordered mechanisms.<sup>47</sup> In addition, substrate inhibition can also be observed in random sequential mechanisms when one substrate has affinity for the binding site of the other.<sup>47</sup> The ping-pong mechanism could be ruled out (Fig. 5). The pattern of lines in the double-reciprocal plot (Fig. 5A) may suggest that recombinant HTP follows a steady-state ordered mechanism, which displays uncompetitive substrate inhibition.<sup>47</sup> However, if HTP followed this mechanism, the pattern of lines for dThd (Fig. 5A) should have been observed for variable  $P_i$  concentrations at fixed-varied dThd concentrations (Fig. 5B). In addition, the double-reciprocal plots should be bent upwards for variable dThd concentrations at fixed-varied  $P_i$  concentrations. This pattern, however, is not observed for dThd (Fig. 5A). Noncompetitive substrate inhibition could be observed for mechanisms in which the inhibitory substrate binds to a second site, an effector site, yielding an inactive enzyme.<sup>48</sup> As shown in TP from mouse liver, noncompetitive substrate inhibition by thymine at high concentrations was based on the binding of thymine to an effector site inhibiting product formation, and a rapid equilibrium random bi-bi mechanism was proposed.<sup>43</sup> Furthermore, the purine riboside derivative KIN59 (5'-*O*-tritylinosine) showed a noncompetitive inhibition against human and *E. coli* TP. Kinetic studies revealed that KIN59 does not compete for the nucleoside or phosphate-binding site of the enzyme.<sup>49</sup> These findings may suggest the existence of an allosteric binding site different from the thymidine and phosphate-binding sites in HTP.

### **Isothermal Titration Calorimetry (ITC) of substrates and products to recombinant HTP**

ITC experiments were thus carried out to ascertain the order of substrate addition and product. Data were best fitted to one binding site model, assuming that ligands bind to dimeric HTP with the same affinity for all active sites. The ITC data for binding of ligands to HTP are summarized in Table 2. The overall binding assays showed that either substrates (dThd and  $P_i$ ) (Fig. 6A and B) or products (thymine and 2dR1P) (Fig. 6C and D) can bind to free HTP enzyme. Although the initial velocity pattern of intersecting lines to the left of the  $y$ -axis (Fig. 5) suggested a sequential mechanism, whether the mechanism followed by HTP is steady-state ordered bi-bi or rapid equilibrium random bi-bi could not be determined. The ITC data demonstrate that the binding of substrates and products to HTP are random (Fig. 6). Accordingly, the reaction catalyzed by HTP follows a rapid-equilibrium random bi-bi kinetic mechanism, in which both substrates can bind to free enzyme to form the catalytically competent ternary complex; and both products can randomly dissociate to yield free enzyme (Fig. 7). This mechanism is in agreement with TP from mouse liver<sup>43</sup>, for which a rapid-equilibrium random bi-bi mechanism has been reported. In contrast, a bi-bi ordered sequential mechanism has been reported for TP from *Escherichia coli*<sup>44</sup> and *Salmonella typhimurium*<sup>45</sup>.

The dThd binding isotherm was not well defined to obtain an adequate stoichiometry value ( $n = 0.2$ ). Nevertheless, for the  $P_i$  binding isotherm, the one binding site model yielded a value of 0.93 for  $n$  (Table 2), suggesting that almost all HTP active sites were occupied by this ligand and that there is one molecule of  $P_i$  bound to each monomer of the homodimeric HTP. This result is consistent with the crystal structure analysis, in which a putative phosphate binding site has been shown in each monomer of HTP, located in the large  $\alpha/\beta$  domain.<sup>39</sup> The ITC data for binding of dThd and  $P_i$  to HTP indicate that they are favorable processes, since the  $\Delta G^\circ$  values for ligand-

macromolecule binary complex formation are negative. The ITC data provide thermodynamic signatures of non-covalent interactions to each binding process.<sup>50</sup> Observed enthalpy changes arise primarily from hydrogen bonding and van der Waals interactions leading to each binary complex formation. The negative sign for  $\Delta H^\circ$  (exothermic process) suggests favorable redistribution of the network of interactions between the substrates (dThd and  $P_i$ ) and HTP, including solvent (Table 2). The favorable entropy (positive  $\Delta S^\circ$ ) observed for  $P_i$  binding to HTP (Table 2) suggests that formation of this binary complex is accompanied by release of "bound" water molecules to the bulk solvent.<sup>50</sup> As a reduction in conformational states in either ligand or protein upon binary complex formation is entropically unfavourable (negative  $\Delta S^\circ$ ), the positive  $\Delta S^\circ$  value for  $P_i$  binding to HTP may also suggest an increase in conformational states.<sup>50</sup> Structural and theoretical studies on *E. coli* TP have suggested that few movements occur after phosphate binding, especially a key hydrogen bond between His119 and Gly208 (His150 and Ala239 in HTP, respectively).<sup>40</sup> In contrast, unfavorable entropy (negative  $\Delta S^\circ$ ) was observed for dThd binding, indicating that binary complex formation may be associated with conformational changes in either the ligand or protein, leading to a reduction in conformational states.<sup>50</sup> This finding is consistent with the crystal structures of HTP, , as either the binding of substrate analogue TPI or thymine can trigger movements of  $\alpha$ -domain and  $\alpha/\beta$ -domain to form the closed (active) conformation of HTP.<sup>26,37</sup>

For both products binding isotherms, the  $n$  value was fixed as one according to the crystal structure analysis, in which a pyrimidine binding site has been observed to each subunit of the homodimeric HTP.<sup>37</sup> The dissociation constant ( $K_d$ ) for 2dR1P is approximately six-fold lower than that of thymine (Table 2). On the other hand, the  $K_d$  value for dThd is three-fold lower than that of the  $P_i$  (Table 2). Interestingly, there

appears to be no energy coupling between the binding of substrates as the  $K_d$  values for  $P_i$  and dThd (Table 2) are in the same range as their  $K_M$  values (Figure 5;  $K_{dThd} = 66 \mu\text{M}$  and  $K_{Pi} = 107 \mu\text{M}$ ). However, it should be pointed out that the Michaelis-Menten constant is not a true dissociation constant; it can, however, be regarded as an apparent dissociation constant that may be treated as the overall dissociation constant of all enzyme-bound species.<sup>41,47</sup> The negative  $\Delta G^\circ$  values for thymine or 2dR1P binding to free HTP show that these processes are favourable as for the dThd and  $P_i$  substrates (Table 2). Interestingly, the binding thermodynamic signatures of 2dR1P binding to HTP (negative  $\Delta H^\circ$  and positive  $\Delta S^\circ$ ) are similar to  $P_i$  (Table 2). On the other hand, similar thermodynamic signatures were observed for dThd substrate and thymine product (Table 2), in which the favorable redistribution of network of interactions upon binary complex formation appears to be accompanied by a reduction in conformational states in either ligand or protein (negative  $\Delta S^\circ$ ). It is tempting to suggest that the latter is likely related to tridimensional conformational changes occurring upon binary complex formation to form the closed active site.<sup>26</sup>

**Table 2.** Thermodynamic parameters of ligands binding to HTP.<sup>a</sup>

Ligands	$n$	$K_a$ ( $\text{M}^{-1}$ )	$\Delta H^\circ$ (kcal mol <sup>-1</sup> )	$\Delta S^\circ$ (cal mol <sup>-1</sup> deg <sup>-1</sup> )	$\Delta G^\circ$ (kcal mol <sup>-1</sup> )	$K_d$ ( $\mu\text{M}$ )
dThd	0.2	$2.1 (\pm 0.4) \times 10^4$	$-1.2 \pm 0.5$	$-20.4 \pm 8.8$	$-6.1 \pm 2.6$	$47 \pm 9$
$P_i$	0.93	$7.0 (\pm 1.6) \times 10^3$	$-3.3 \pm 1.1$	$7.0 \pm 2.3$	$-5.5 \pm 1.8$	$142 \pm 32$
Thymine	1	$6.4 (\pm 0.6) \times 10^3$	$-7.1 \pm 0.3$	$-5.4 \pm 0.5$	$-5.4 \pm 0.5$	$155 \pm 9$
2dR1P	1	$4.4 (\pm 1.0) \times 10^4$	$-4.0 \pm 0.2$	$8.2 \pm 1.9$	$-6.6 \pm 1.6$	$23 \pm 5$

<sup>a</sup> $n$  = number of sites,  $K_a$  = association constant;  $\Delta H^\circ$  = binding enthalpy,  $\Delta S^\circ$  = binding

entropy,  $\Delta G^\circ$  = Gibbs free energy,  $K_d$  = dissociation constant.

### pH-rate profiles

The pH dependence of  $k_{cat}$  and  $k_{cat}/K_M$  for dThd and  $P_i$  were determined to probe acid/base chemistry in HTP mode of action. The pH-rate profiles (Fig. 8) were bell-

shaped for  $k_{\text{cat}}/K_{\text{dThd}}$  (Fig. 8B) and  $k_{\text{cat}}/K_{\text{Pi}}$  (Fig. 8C) analysis, and the data were thus fitted to Eq. (8). The bell-shaped pH-rate profiles showed slope values of + 1 for the acidic limb and – 1 for the basic limb, indicating participation of a single ionizable group in each limb (Fig. 8B and Fig. 8C). The data from pH 5.5 for  $k_{\text{cat}}/K_{\text{Pi}}$  were not included in the analysis as the saturation curve was sigmoidal rather than hyperbolic.

The pH-rate profile for  $k_{\text{cat}}$  shows an increase in catalytic rate at low pH values (Fig. 8A). Although the enzyme has shown the maximal activity at low pH, the substrate affinities were reduced at both low and high pHs (Fig. 8B and Fig. 8C). Notwithstanding, the pH dependence of  $k_{\text{cat}}$  (Fig. 8A) could not be fitted to the bell-shaped pH-rate equation or to other usually observed pH-rate profiles.<sup>47</sup> It could be argued that the pH-rate profile for  $k_{\text{cat}}$  (Fig. 8A) suggests a linear portion with slope of – 1 between low and large pH values, in which there would be, respectively, optimum enzyme activity and partial HTP activity (two apparent pKs). However, the data (Fig. 8A) are poorly defined and no reliable estimates could be obtained. In any case, the rather unusual dependence of  $k_{\text{cat}}$  on pH values suggests that HTP catalysis is more favorable with protonation of an amino acid residue and its unprotonation is detrimental to enzyme catalysis. Targeted molecular dynamics results suggest that in doubly protonated His85 of *E. coli* TP (His116 for HTP), the  $\delta 1$  (N-1) proton is hydrogen bonded to the phosphate and the  $\epsilon 2$  (N-3) proton could be involved in protonation of O-2 of thymidine.<sup>51</sup> On the other hand, it has been proposed that His116 plays a role in either stabilizing the transition state during catalysis or in donating a proton to the N-1 of the pyrimidine ring following glycosidic cleavage.<sup>26</sup> Crystal structure of HTP in complex with the small inhibitor TPI showed its participation in a proton shuttling mechanism, where Asp114, Glu225 and Lys222 form a triad delivering proton to His116.<sup>26</sup> Mutational studies of His116 to a phenylalanine or a lysine revealed a severe

effect on HTP as both mutations completely abolish the enzymatic activity.<sup>38</sup> In addition, it has been pointed that the optimum pH for dThd cleavage was close to 5.5,<sup>52</sup> and the maximal activity of the enzyme was at pHs 6.0 and 6.3 for, respectively, *Lactobacillus casei* TP<sup>46</sup> and *E. coli* TP.<sup>44</sup> However, the results here presented cannot provide any  $pK_a$  value for  $k_{cat}$ , at most they indicate that the maximal rate activity was achieved at low pH.

The pH-rate profile for  $k_{cat}/K_{dThd}$  indicates that protonation of a group with  $pK_a$  of 5.2 ( $\pm 0.5$ ) and deprotonation of a group with  $pK_a$  of 9.0 ( $\pm 0.8$ ) abolish the ability of dThd to bind and react (Fig. 8B). Crystal structures of HTP in complex with the small molecule inhibitor TPI,<sup>26</sup> the natural product thymine,<sup>37</sup> and the substrate 5-iodouracil (5IUR)<sup>38</sup> demonstrate that the side chain of His116 is located in the HTP pyrimidine binding site, which is, in turn, the thymidine binding site. His116 belongs to the  $\alpha/\beta$  domain of the HTP active site where is located the phosphate binding site, and hydrogen bonds are made between TPI/thymine/5IUR and this residue. The thymine binding is similar to the 5-chlorouracil of TPI, in which the methyl group of thymine was replaced with chlorine. Moreover, His116 directly interacts with 5IUR via its  $\epsilon 2$  (N-3) group. The structural analysis of *Bacillus stearothermophilus* PyNP in complex with the substrate analogue pseudouridine in its active site showed that His82 (His116 in HTP) makes a hydrogen-bonding network with the uracil moiety of the substrate analogue.<sup>40</sup> Given these observations, the side chain of His116 seems to be a likely candidate for the group with  $pK_a$  value of 5.1 that must be unprotonated to interact with dThd in HTP active site. Accordingly, His116 appears to be important not only to enzyme catalysis but also for substrate binding. The crystal structures have also demonstrated that the side chain of Lys221 interacts directly with TPI/thymine/5IUR through hydrogen bonds. Differently to His116, Lys221 belongs to the  $\alpha$  domain, in which the pyrimidine binding

site is located, as the other residues that are involved in TPI/thymine/5IUR binding. It suggests that the side chain of Lys221 is a likely candidate for a group with  $pK_a$  value of 9.0 that must be protonated for pyrimidine binding to occur. Although none of the HTP crystal structures solved to date is in complex with the natural substrate thymidine and there are no data showing the amino acid residues involved in the interaction between HTP and thymidine, the results here presented suggest that Lys221 is likely to interact with dThD in a similar manner as shown for TPI/thymine/5IUR.<sup>26,37,38</sup>

The pH-rate profile for  $k_{cat}/K_{P_i}$  indicates that a group with  $pK_a$  of 6.1 ( $\pm 0.6$ ) must be unprotonated and a group with  $pK_a$  of 7.8 ( $\pm 0.8$ ) must be protonated for  $P_i$  binding to occur. The side chain of Lys81 has been shown to be involved in *Bacillus stearothermophilus* PyNP phosphate binding site,<sup>40</sup> corresponding to Lys115 in HTP. Besides, the side chain of Lys84 has been proposed as putative phosphate binding site in *E. coli* TP,<sup>39</sup> corresponding to Lys115 in HTP. It is thus tempting to suggest that  $\epsilon$ -amino group of Lys115 is a likely candidate for the residue with a  $pK_a$  value of 7.8 ( $\pm 0.8$ ) whose protonation abolishes phosphate binding. The pH-rate data are in agreement with site-directed mutagenesis and kinetic analysis, showing that lysates of Lys115Glu HTP mutant expressed in COS cells have no detectable HTP activity.<sup>12</sup> The bell-shaped pH profile for  $k_{cat}/K_{P_i}$  also showed participation of a single ionizable group with  $pK_a$  of 6.1 ( $\pm 0.6$ ) that has to be unprotonated for  $P_i$  binding. Although the other amino acid residues reported to be involved in  $P_i$  binding do not have ionizable side chains, it is possible that the group with a  $pK_a$  value of 6.1 is an ionizable group of phosphate.

## Conclusions

As HTP is a key enzyme involved in pyrimidine metabolism and its activity appears to be essential for angiogenesis in certain tumors, the biochemical studies on HTP mode of action are thus worth pursuing. Interest in HTP inhibitors has been considerably renewed in the last years and different strategies have been followed to design new and potent inhibitors. Inhibition of the enzyme activity has been investigated as a chemotherapeutic strategy to decrease angiogenesis, slow tumor growth, and reduce metastasis.<sup>6</sup> In addition, inhibitors of HTP could be useful since tumors depend on the nucleotide salvage pathway for their proliferation.<sup>53</sup> The most potent and effective inhibitors take advantage of enzyme chemistry to achieve inhibition. The catalytic chemistry of enzymes is the key to designing potent inhibitors and makes them a special class of drug targets.<sup>54</sup> Mechanistic analysis should thus be a top priority for enzyme-targeted drug design programs.

Here, we present an efficient method to obtain homogeneous recombinant HTP. Initial velocity and isothermal calorimetry studies demonstrated that HTP follows a rapid-equilibrium random bi-bi kinetic mechanism. Amino acid residues involved in substrate binding were proposed based on pH-rate profiles, suggesting that the His116 and Lys221 side chains appear to be essential for dThd binding, and the side chain of Lys115 appears to be essential for P<sub>i</sub> binding. Maximal HTP rate activity was achieved at low pH values. An improved understanding of the mode of action of HTP may be useful to medicinal chemists and chemical biologists. The former would benefit from an improved understanding of HTP mode of action to design potent enzyme inhibitors to be tested as chemotherapeutic agents, and the latter would be interested in these

compounds to carry out loss-of-function experiments to reveal the biological role of HTP in angiogenesis and other biological processes such as apoptosis and metastasis.

## Experimental procedures

### Tissue sample

A single specimen of colorectal tumor tissue was obtained from a patient who underwent surgical treatment at the Hospital São Lucas, Pontifical Catholic University of Rio Grande do Sul (PUCRS) in agreement with the purpose of the study. The research project was approved by Human Studies and Ethics (CEP) under protocol number 11/05429.

### Gene amplification and cloning

The *TYMP* gene (NM\_001953.4) was PCR amplified from the cDNA synthesized by RT-PCR amplification of total RNA isolated from colorectal tumor specimen as previously described.<sup>55</sup> The synthetic oligonucleotides used for amplification of the coding sequence (residues 11 – 482) (forward primer, 5'-GAC ATA TGG CCC CAC CCG CGC CTG GTG ACT T-3'; and reverse primer, 3'-AAA AGC TTT CAT TGC TGC GGC GGC AGA ACG AGC-5') were designed to contain, respectively, *NdeI* and *HindIII* (New England Biolabs) restriction sites (underlined). The DNA fragment was amplified using *Pfu* DNA polymerase in the presence of 5% dimethyl sulfoxide (DMSO; final concentration). The PCR product was detected on 1% agarose gel, and a 1415-bp band was purified utilizing the Quick Gel Extraction Kit (Invitrogen). The purified fragment was cloned into pCR-Blunt® vector (Invitrogen) and, subsequently, subcloned into pET-23a(+) expression vector (Novagen), previously digested with *NdeI* and *HindIII* restriction enzymes. The coding *TYMP* gene sequence was determined by automated DNA sequencing to confirm sequence identity and the absence of mutations in the cloned fragment.

## Expression, purification and absorption coefficient determination of recombinant HTP

The pET-23a(+):*TYMP* recombinant plasmid was transformed into *E. coli* Rosetta (DE3) competent cells (Novagem) and selected on Luria-Bertani (LB) agar plates containing  $50 \mu\text{g mL}^{-1}$  ampicillin and  $34 \mu\text{g mL}^{-1}$  chloramphenicol. A single colony was grown in 50 mL of LB medium containing the same antibiotics at 37°C. Aliquots of this culture (12 mL) was used to inoculate Terrific Broth (TB) medium (4 x 500 mL, containing the same antibiotics) and grown for 24 h at 37°C and 180 rpm after reaching an  $\text{OD}_{600\text{nm}}$  0.4 – 0.6. Recombinant HTP protein expression was achieved without IPTG induction. The cells (29 g) were collected by centrifugation at 11,800 g for 30 min at 4°C and stored at – 20°C. The same procedure was employed for *E. coli* Rosetta (DE3) cells transformed with pET-23a(+) without the *TYMP* gene as negative control. The expression of soluble and insoluble protein was confirmed by 12% SDS – PAGE stained with Coomassie Brilliant Blue.<sup>56</sup>

All purification steps were performed using an ÄKTA system (GE Healthcare) in a cold room at 4°C, and protein elution was monitored by UV detection. Approximately 7.6 g of frozen cells were resuspended in 76 mL of 50 mM Tris pH 7.5 (buffer A) and incubated with  $0.2 \text{ mg mL}^{-1}$  of lysozyme (Sigma – Aldrich) for 30 min with stirring. The cells were disrupted by sonication with 10 pulses of 10 s each at 60% amplitude with 13 mm probe, and centrifuged at 48,000 g for 30 min to remove cell debris. The supernatant was treated with 1% (wt/vol) streptomycin sulfate (Sigma – Aldrich), stirred for 30 min to precipitate nucleic acids, and centrifuged at 48,000 g for 30 min. The resulting supernatant containing the soluble HTP was dialyzed against buffer A 3 x 2 L (2.5 h each), and clarified by centrifugation at 48,000 g for 30 min. The sample was loaded on an anion exchange chromatographic column ( Q-Sepharose Fast

Flow, GE Healthcare), pre-equilibrated with buffer A, washed with 5 column volumes (CV) of buffer A, and proteins were eluted with 20 CV linear gradient (0 – 100%) of 50 mM Tris 500 mM NaCl pH 7.5 (buffer B) at a 1 mL min<sup>-1</sup> flow rate. All fractions were analyzed by 12% SDS – PAGE stained with Coomassie Brilliant Blue, and the fractions containing the recombinant enzyme were pooled and dialyzed against 3 x 2 L (2.5 h each) of buffer A. Ammonium sulfate was added to the dialyzed fractions to a final concentration of 700 mM, and centrifuged at 48,000 g for 30 min. The supernatant was loaded on a hydrophobic interaction chromatographic column (HiLoad Phenyl Sepharose High performance, GE Healthcare), pre-equilibrated with 50 mM Tris 700 mM (NH<sub>4</sub>)<sub>2</sub>SO<sub>4</sub> pH 7.5 (buffer C). The column was washed with 5 CV of buffer C, and proteins were eluted with 20 CV linear gradient (0 – 100%) of buffer A at a 1 mL min<sup>-1</sup> flow rate, yielding homogeneous HTP recombinant protein, as inferred by 12% SDS – PAGE stained with Coomassie Brilliant Blue. The eluted fractions were dialyzed against buffer A 3 x 2 L (2.5 h each) and stored at – 80°C. Pooled fractions of all purification steps were analyzed by 12% SDS – PAGE stained with Coomassie Brilliant Blue. Protein concentration was determined either by the method of Bradford<sup>57</sup> or by direct absorbance measurement. A value of 29,512 M<sup>-1</sup> cm<sup>-1</sup> for the molar absorption coefficient at 280 nm ( $\epsilon_{280\text{nm}}$ ) of HTP in buffer A at 37°C was determined using the method of Edelhoich.<sup>58,59</sup>

### **Determination of HTP molecular mass by MS**

Intact protein analysis was performed by direct injection of HTP samples (reconstituted in acetonitrile 50%: water 49.8%: formic acid 0.2%) into an IonMax electrospray ion source. We applied 4.5 kV in positive ion mode, 200 °C of capillary temperature and 110 V of tube lens voltage. High-resolution spectra (120-2000 m/z range) were

collected in FTMS mode using an Orbitrap analyzer (Thermo Discovery XL) at a nominal resolution of 30,000. Charge state deconvolution of averaged data from 417 spectra were performed using the software MagTran.<sup>60</sup>

### **Primary structure analysis of HTP by mass spectrometry (MS)**

Samples of purified HTP (1 nmol) were trypsin digested using a protocol adapted from Klammer & MacCoss (2006).<sup>60</sup> The resulting peptide mixtures were subjected to nanochromatography (nanoLC Ultra 1D plus - Eksigent, USA) using a home-made capillary column (15 cm in length, 150  $\mu\text{m}$  i.d., Kinetex C18 core-shell particles – Phenomenex, Inc.). The eluted peptides were detected using an LTQ-Orbitrap hybrid mass spectrometer (Thermo Electron Corporation). MS/MS fragmentation was performed using collision-induced dissociation (CID) with an activation Q of 0.250, an activation time of 30.0 ms, and an isolation width of 1.0 Da. The searches were performed against the human proteome. We allowed a precursor tolerance of 10 ppm, a fragment tolerance of 0.8 Da, static carbamidomethylation on cysteines, and dynamic oxidation on methionine residues.

### **Determination of oligomeric state of HTP in solution**

The molecular mass of recombinant HTP was determined by gel filtration chromatography using a Superdex 200 HR 10/30 (GE Healthcare) size exclusion column, pre-equilibrated with 50 mM Tris pH 7.5 buffer, containing 200 mM NaCl, and a flow rate of 0.4 mL min<sup>-1</sup>. The LMW and HMW Gel filtration Calibrations Kits (GE Healthcare) were used as the protein mass molecular standards in the calibration curve construction. The elution volumes ( $V_e$ ) of protein standards (ferritin, catalase, aldolase, coalbumin, ovoalbumin, ribonuclease A) were used to calculate their corresponding

partition coefficient ( $K_{AV}$ ) according to Eq. (1). Blue dextran 2000 (GE Healthcare) was used to determine the void volume ( $V_0$ ) and  $V_t$  is the total bead volume of the column. The  $K_{AV}$  value for each standard protein was plotted against the logarithm of their molecular mass, yielding a linear function with values for the  $y$ -intercept and the slope given in Eq. (2). The partition coefficient ( $K_{AV}$ ) of the recombinant HTP was calculated by data fitting to Eq. (1). Protein elution was monitored at 215, 254, and 280 nm.

$$K_{AV} = \frac{V_e - V_0}{V_t - V_0} \quad \text{Eq. (1)}$$

$$K_{AV} = 0.9669 - 0.3087 \log(kDa) \quad \text{Eq. (2)}$$

### HTP enzymatic assay

All chemicals in enzyme activity measurements were purchased from Sigma Aldrich. HTP activity was measured for all purification steps in the forward direction, using a continuous spectrophotometric rate assay in a 1.0 cm path length quartz cuvette on a UV-2550 UV/Vis spectrophotometer (Shimadzu). All activity assays were performed using 67 nM of homogenous HTP in 50 mM Tris pH 7.5, varying concentrations of thymidine (dThd) and phosphate ( $P_i$ ) at 37°C for 60 s in a final volume of 0.5 mL. The reaction progress was monitored by the decrease in absorbance upon conversion of dThd to thymine at 290 nm. The molar absorption extinction coefficient at 290 nm ( $\epsilon_{290\text{nm}}$ ) was determined under the standard assay conditions by direct absorbance measurements. A value of 2,000  $\text{M}^{-1} \text{cm}^{-1}$  for the molar absorption coefficient at 290 nm ( $\epsilon_{290\text{nm}}$ ) was determined by the difference in the molar extinction coefficient between dThd and thymine and it was employed to calculate the rate of HTP-catalyzed chemical

reaction. One unit (U) of enzyme activity was defined as the amount of enzyme that converts 1  $\mu\text{mol}$  each of dThd and  $\text{P}_i$  to thymine and 2dR1P per minute at pH 7.5 at 37°C.

### Determination of apparent steady-state kinetic constants and initial velocity patterns

To determine the apparent steady-state kinetic constants, HTP activity was monitored at varying concentrations of dThd (50 – 900  $\mu\text{M}$ ) and fixed-saturating concentration of  $\text{P}_i$  (2 mM), and at varying concentration of  $\text{P}_i$  (100 – 1000  $\mu\text{M}$ ) and a fixed-saturating concentration of dThd (400  $\mu\text{M}$ ) under the standard condition assay. The data were either fitted by non-linear regression analysis to the Michaelis-Menten equation<sup>41</sup> (Eq. (3)) for a hyperbolic saturation curve, or to the substrate inhibition equation<sup>47</sup> (Eq. (4)) in which  $v$  is the steady-state velocity,  $V_{\text{max}}$  is the maximal rate,  $S$  is the substrate concentration,  $K_M$  is the Michaelis constant, and  $K_i$  is the dissociation constant for substrate inhibition. The  $k_{\text{cat}}$  values were calculated from Eq. (5).<sup>41</sup>

$$v = \frac{V_{\text{max}}[S]}{K_M + [S]} \quad \text{Eq. (3)}$$

$$v = \frac{V_{\text{max}}[S]}{K_M + [S] \left( 1 + \frac{[S]}{K_i} \right)} \quad \text{Eq. (4)}$$

$$k_{\text{cat}} = \frac{V_{\text{max}}}{[E]_t} \quad \text{Eq. (5)}$$

To determine the true steady-state kinetic parameters and the enzyme kinetic mechanism (patterns in double-reciprocal plots) for dThd and P<sub>i</sub>, initial velocity measurements were carried out in duplicates for varying one substrate concentrations in the presence of fixed-varied concentrations of the other substrate. Accordingly, saturating curves were performed in the presence of varying concentrations of dThd (50, 100, 200, 300, and 500 μM) at several fixed-varied concentrations of P<sub>i</sub> (70, 100, 150, 200, 400, and 1000 μM). Data from initial velocity double reciprocal plots of lines intersecting to the left of the *y*-axis were fitted to Eq. (6), which describes a mechanism involving ternary complex formation and sequential substrate binding,<sup>41</sup> using SigmaPlot 10 Software.

$$v = \frac{VAB}{K_{ia}K_b + K_aB + K_bA + AB} \quad \text{Eq. (6)}$$

For Eq. (6), *v* is the measured steady-state velocity, *V* is the maximal velocity, *A* and *B* are the concentrations of the substrates (dThd and P<sub>i</sub>), *K<sub>a</sub>* and *K<sub>b</sub>* are their respective Michaelis constant, and *K<sub>ia</sub>* is the dissociation constant for enzyme-substrate A binary complex formation.

### **Isothermal Titration Calorimetry (ITC)**

Ligand binding assays were carried out using the iTC200 Microcalorimeter (Microcal, Inc., Northampton, MA). Reference cell (200 μL) was loaded with Milli Q water during all experiments and the sample cell (200 μL) was filled with recombinant HTP at a concentration of 88 μM or 104 μM, in buffer A. The same buffer was used to prepare all solutions of ligands. The injection syringe (39,7 μL) was filled with substrates or products at different concentrations (dThd 1 mM, P<sub>i</sub> 3 mM, Thymine 5 mM, and 2dR1P

3.5 mM) and the ligand bindings were measured by direct titration of ligand into macromolecule. The stirring speed was 500 rpm and the temperature was set to 37°C for all binding experiments. The first injection (0.5  $\mu\text{L}$ ) was discarded in the data analysis and was followed by 19 injections of 2.0  $\mu\text{L}$  each, at 180 s intervals. Control titrations (ligand into buffer A) were performed to subtract the heats of dilution and mixing for each experiment prior to data analysis. ITC was employed to determine the binding of ligands to free HTP, measuring the amount of heat generated or consumed upon binary complex formation, at constant temperature and pressure. ITC data were evaluated using the Origin 7 SR4 software (Microcal, Inc). All data were fitted to Eq. (7), in which  $\Delta H^\circ$  is the enthalpy of binding,  $\Delta G^\circ$  is the Gibbs free energy change,  $\Delta S^\circ$  is the entropy change,  $T$  is the absolute temperature in Kelvin,  $R$  is the gas constant (1.987 cal  $\text{K}^{-1} \text{mol}^{-1}$ ), and  $K_a$  is the equilibrium association constant. The initial estimates for  $n$ ,  $K_a$  and  $\Delta H^\circ$  parameters were provided in the software by standard Marquardt non-linear regression method. The equilibrium dissociation constant,  $K_d$ , was calculated as the inverse of  $K_a$ .

$$\Delta G^\circ = -RT \ln K_a = \Delta H^\circ - T\Delta S^\circ \quad \text{Eq. (7)}$$

### pH-rate profiles

The dependence of kinetic parameters on pH was determined by measuring initial velocities in the presence of varying concentrations of one substrate at saturating level of the other, in a buffer mixture of 500 mM 2-(*N*-morpholino)-ethanesulfonic acid (MES)/*N*-(2-hydroxyethyl)piperazine-*N'*-2-ethanesulfonic acid (HEPES)/2-(*N*-cyclohexylamino)-ethanesulfonic acid (CHES) over the following pH values: pH 5.5, 6.0, 6.5, 7.0, 7.5, 8.0, 8.5, and 9.0.<sup>47</sup> As the  $K_M$  values changed as a function of pH,

different concentration ranges of the variable substrate and the fixed substrate were employed. For all pH tested, 40 nM of recombinant HTP was used in a final volume of 0.5 mL, except at pH 9.0, in which the final enzyme concentration was 80 nM when dThd was the fixed substrate due to low activity. The experimental conditions were as follows: at pH 5.5 (50 – 600  $\mu$ M varying dThd concentration and fixed concentration of  $P_i$  at 10 mM, and 2 – 10 mM varying  $P_i$  concentration and fixed concentration of dThd at 500  $\mu$ M), pH 6.0 (30 – 500  $\mu$ M varying dThd concentration and fixed concentration of  $P_i$  at 5 mM, and 100 – 5000  $\mu$ M varying  $P_i$  concentration and fixed concentration of dThd at 400  $\mu$ M), pH 6.5 (30 – 500  $\mu$ M varying dThd concentration and fixed concentration of  $P_i$  at 2 mM, and 50 – 1800  $\mu$ M varying  $P_i$  concentration and fixed concentration of dThd at 400  $\mu$ M), pH 7.0 (30 – 300  $\mu$ M varying dThd concentration and fixed concentration of  $P_i$  at 2 mM, and 50 – 1600  $\mu$ M varying  $P_i$  concentration and fixed concentration of dThd at 300  $\mu$ M), pH 7.5 (30 – 400  $\mu$ M varying dThd concentration and fixed concentration of  $P_i$  at 2 mM, and 50 – 1600  $\mu$ M varying  $P_i$  concentration and fixed concentration of dThd at 300  $\mu$ M), pH 8.0 (30 – 300  $\mu$ M varying dThd concentration and fixed concentration of  $P_i$  at 2 mM, and 50 – 1800  $\mu$ M varying  $P_i$  concentration and fixed concentration of dThd at 300  $\mu$ M), pH 8.5 (30 – 300  $\mu$ M varying dThd concentration and fixed concentration of  $P_i$  at 3 mM, and 100 – 1600  $\mu$ M varying  $P_i$  concentration and fixed concentration of dThd at 300  $\mu$ M), and pH 9.0 (30 – 400  $\mu$ M varying dThd concentration and fixed concentration of  $P_i$  at 10 mM, and 1 – 8 mM varying  $P_i$  concentration and fixed concentration of dThd at 300  $\mu$ M).

The data for pH-rate profiles data for  $\log k_{cat}/K_M$  were fitted to Eq. (8) using SigmaPlot 10 Software. This equation describes a bell-shaped pH profile for a single ionizable group (slope of 1 for the acidic limb) that must be unprotonated for binding/catalysis and another single ionizable group (slope of - 1 for the basic limb) that

must be protonated for binding/catalysis to occur. For Eq. (8),  $y$  is the kinetic parameter,  $C$  is the pH-independent value of  $y$ ,  $H$  is the hydrogen ion concentration, and  $K_a$  and  $K_b$  are, respectively, the apparent acid and base dissociation constants for ionizing groups.<sup>47</sup>

$$\log y = \log \left( \frac{C}{1 + \frac{H}{K_a} + \frac{K_b}{H}} \right) \quad \text{Eq. (8)}$$

## Acknowledgements

This work was supported by funds awarded by Decit/SCTIE/MS-MCT-CNPq-FNDCT-CAPES to National Institute of Science and Technology on Tuberculosis (INCT-TB) to D.S.S. and L.A.B. L.A.B. and D.S.S. also acknowledge financial support awarded by FAPERGS-CNPq-PRONEX-2009. L.A.B. (CNPq, 520182/99-5) and D.S.S. (CNPq, 304051/1975-06) are Research Career Awardees of the National Research Council of Brazil (CNPq). L.K.B.M is a post-doctoral fellow of CNPq/FAPERGS. C.D acknowledges a PhD scholarship awarded by CAPES and D.C.R. acknowledges a PhD scholarship awarded CNPq.

## References

- 1 M.J. Pugmire, S.E. Ealick, *Biochem. J.*, 2002, **361**, 1-25.
2. Friedkin M, Roberts D, *J. Biol. Chem.*, 1954, **207**, 245-256.
- 3 K. Usuki, J. Saras, J. Waltenberger, K. Miyazono, G. Pierce, A. Thomason and C. H. Heldin, *Biochem. Biophys. Res. Commun.*, 1992, **184**, 1311-1316.
- 4 L. Griffiths and I. J. Stratford, *Br. J. Cancer*, 1997, **76**, 689-693.
- 5 C. H. Heldin, K. Usuki and K. Miyazono, *J. Cell. Biochem.*, 1991, **47**, 208-210.
- 6 A. Bronckaers, F. Gago, J. Balzarini and S. Lienkens, *Med. Res. Rev.*, 2009, **29**, 903-953.
- 7 T. A. Krenitsky, *J. Biol. Chem.*, 1968, **243**, 2871-2875.
- 8 M. Schwartz, *Eur. J. Biochem.*, 1971, **21**, 191-198.
- 9 I. V. Bijnsdorp, M. de Bruim, A. C. Laan, M. Fukushima and G. J. Peters, *Nucleos. Nucleot. Nucl.*, 2008, **27**, 681-691.
- 10 F. Fochoer and S. Spadari, *Curr. Cancer Drug. Targets*, 2001, **1**, 141-153
- 11 A. Moghaddam, H. T. Zhang, T. P. Fan, D. E. Hu, V. C. Lees, H. Turley, S. B. Fox, K. C. Gatter, A. L. Harris and R. Bicknell, *Proc. Natl. Acad. Sci. USA*, 1995, **92**, 998-1002.
- 12 K. Miyadera, T. Sumizawa, M. Haraguchi, H. Yoshida, W. Konstanty, Y. Yamada and S. Akiyama, *Cancer Res.*, 1995, **55**, 1687-1690.
- 13 T. Sumizawa, T. Furukawa, M. Haraguchi, A. Yoshimura, A. Takeyasu, M. Ishizawa, Y. Yamada and S. Akiyama S, *J. Biochem.*, 1993, **114**, 9-14.
- 14 K. A. Hotchkiss, A. W. Ashton and E. L. Schwartz, *J. Biol. Chem.*, 2003, **278**, 19272-19279.

- 15 M. de Bruin, K. Smid, A. C. Laan, P. Noordhuis, M. Fukushima, K. Hoekman, H. M. Pinedo and G. J. Peters, *Biochem. Biophys. Res. Commun.*, 2003, **301**, 675-679.
- 16 C. Desgranges, G. Razaka, M. Rabaud and H. Bricaud, *Biochem. Biophys. Acta*, 1981, **654**, 211-218.
- 17 I. V. Bijnsdorp, K. Azijli, E. E. Jansen, M. M. Wamelink, C. Jakobs C, E. A. Struys, M. Fukushima, F. A. Kruyt and G. J. Peters, *Biochem. Pharmacol.*, 2010, **80**, 786-792.
- 18 M. J. Pérez-Pérez, E. M. Priego, A. I. Hernández, M. J. Camarasa, J. Balzarini and S. Liekens, *Mini Rev. Med. Chem.*, 2005, **5**, 1113-1123.
- 19 C. Cole, A. J. Foster, S. Freeman, M. Jaffar, P. E. Murray and I. J. Stratford, *Anticancer Drug. Des.*, 1999, **14**, 383-392.
- 20 S. Akiyama, T. Furukawa, T. Sumizawa, Y. Takebayashi, Y. Nakajima, S. Shimaoka and M. Haraguchi, *Cancer Sci.*, 2004, **95**, 851-857.
- 21 M. Toi, R. M. Atiqur, H. Bando and L. W. Chow, *Lancet Oncol.*, 2005, **6**, 158-166.
- 22 S. Matsushita, T. Nitanda, T. Furukawa, T. Sumizawa, A. Tani, K. Nishimoto, S. Akiba, K. Miyadera, M. Fukushima, Y. Yamada, H. Yoshida, T. Kansaki and S. Akiyama, *Cancer Res.*, 1999, **59**, 1911-1916.
- 23 M. L. Price, W. C. Guida, T. E. Jackson, J. A. Nydick, P. L. Gladstone, J. C. Juarez, F. Doñate and R. J. Ternansky, *Bioorg. Med. Chem. Lett.*, 2003, **13**, 107-110.
- 24 P. Reigan, A. Gbaj, E. Chinje, I. J. Stratford, K. T. Douglas and S. Freeman, *Bioorg. Med. Chem. Lett.*, 2004, **14**, 5247-5250.
- 25 M. Rajabi, D. Mansell, S. Freeman and R. A. Bryce, *Eur. J. Med. Chem.*, 2011, **46**, 1165-1171.
- 26 R. A. Normam, S. T. Barry, M. Bate, J. Breed, J. G. Colls, R. J. Ernill, R. W. Luke, C. A. Minshull, M. S. McAlister, E. J. McCall, H. H. McMiken, D. S. Paterson, D. Timms, J. A. Turcker and R. A. Pauptit, *Structure*, 2004, **12**, 75-84.

- 27 V.A. McNally, A. Gbaj, K T. Douglas, I. J. Stratford, M. Jaffar, S. Freeman and R. A. Bryce, *Bioorg. Med. Chem. Lett.*, 2003, **13**, 3705-3709.
- 28 M. R. Birck and V. L. Schramm, *J. Am. Chem. Soc.*, 2004, **126**, 2447-2453.
- 29 P. A. Schwartz, M. J. Veticatt and V. L. Schramm, *J. Am. Chem. Soc.*, 2010, **132**, 13425-13433.
- 30 P.R. Winship, *Nucleic. Acids Res.*, 1989, **17**, 1266.
- 31 K. Hagiwara, G. Stenman Honda, P. Sahlin, A. Andersson, K. Miyazono, C. H. Heldin, F. Ishikawa and F. Takaku, *Mol. Cell. Biol.*, 1991, **11**, 2125-2132.
- 32 D. Renck, R. G. Ducati, M. S. Palma, D. S. Santos and L. A. Basso, *Arch. Biochem. Biophys.*, 2010, **497**, 35-42.
- 33 L. K. B. Martinelli, R. G. Ducati, L. A. Rosado, A. Breda, B. P. Selbach, D. S. Santos and L. A. Basso, *Mol. Biosyst.*, 2011, **7**, 1289-1305.
- 34 K. C. Kelley, K. J. Huestis, D.A. Austen, C. T. Sanderson, M. A. Donohue, S. K. Stickel, E. S. Kawasaki and M. S. Osburne, *Gene*, 1995, **156**, 33-36.
- 35 T. H. Grossman, E. S. Kawasaki, S. R. Punreddy and M. S. Osburne, *Gene*, 1998, **209**, 95-103.
- 36 F. W. Studier, *Protein. Expr. Purif.*, 2005, **41**, 207-234.
- 37 K. el Omari, A. Bronckaers, S. Lienkens, M. J. Pérez-Pérez, J. Balzarini and D. K. Stammers, *Biochem. J.*, 2006, **399**, 199-204.
- 38 E. Mitsiki, A. C. Papageorgiou, S. Iyer, N. Thiyagarajan, S. H. Prior, D. Sleep, C. Finnis and K. R. Acharya, *Biochem. Biophys. Res. Commun.*, 2009, **386**, 666-670.
- 39 M. R. Walter, W. J. Cook, L. B. Cole, S. A. Short, G. W. Koszalka, T. A. Krenitsky and S. E. Ealick, *J. Biol. Chem.*, 1990, **265**, 14016-14022.
- 40 M. J. Pugmire and S. E. Ealick, *Structure*, 1998, **6**, 1467-1479.

- 41 I. H. Segel, *Enzyme Kinetics – Behavior and analysis of rapid equilibrium and steady-state enzyme systems*, John Wiley & Sons, Inc., New York, 1975, 957p.
- 42 T. W. Traut, *Mol. Cell. Biochem*, 1994, **140**, 1-22.
- 43 M. H. Iltzsch, M. H. el Kouni and S. Cha S, *Biochemistry*, 1985, **24**, 6799-6807.
- 44 M. Schwartz, *Eur. J. Biochem.*, 1971, **21**, 191-198.
- 45 J. G. Blank and P. A. Hoffee, *Arch. Biochem. Biophys.*, 1975, **168**, 259-265.
- 46 Y. Avraham, N. Grossowicz and J. Yashphe, *Biochem. Biophys. Acta*, 1990, **1040**, 287-293.
- 47 P. F. Cook and W. W. Cleland, *Enzyme Kinetics and Mechanism*, Garland Science Publishing, New York, 2007, 404p.
- 48 I. J. MacRae and I. H. Segel, *Arch. Biochem. Biophys.*, 1999, **361**, 277-282.
- 49 S. Liekens, A. I. Hernández, D. Ribatti, E. De Clercq, M. J. Camarasa, M. J. Pérez-Pérez and J. Balzarini, *J. Biol. Chem.*, 2004, **279**, 29598-29605.
- 50 J. E. Ladbury and M. L. Doyle, in *Biocalorimetry II*, ed. Wiley, London, 1st ed., 2004, 259.
- 51 J. Mendieta, S. Martín-Santamaría, E. M. Priego, J. Balzarini, M. J. Camarasa, M. J. Pérez-Pérez and F. Gago, *Biochemistry*, 2004, **43**, 405-414.
- 52 T. A. Krenitsky, J. W. Mellors and R. K. Barclay. *J. Biol. Chem.*, 1965, **240**, 1281-286.
- 53 P. M. Schwartz and L. M. Milstone, *Biochem. Pharmacol.*, 1988, **37**, 353-355.
- 54 J. G. Robertson, *Curr. Opin. Struct. Biol.*, 2007, **17**, 674-679.
- 55 C. Deves, D. Renck, B. Garicochea, V. D. da Silva, T. G. Lopes, H. Fillman, L. Fillman, S. Lunardini, L. A. Basso, D. S. Santos and E. L. Batista Jr., *Virchows Arch.*, 2011, **4**, 421-430.
- 56 U.K. Laemmli, *Nature*, 1970, **227**, 680-685.

57 M. M. Bradford, *Anal. Biochem.*, 1976, **72**, 248-254.

58 H. Edelhoch, *Biochemistry*, 1967, **6**, 1948-1954.

59 C. N. Pace, F. Vjados, L. Fee, G. Grimsley and T. Gray, *Protein Sci.*, 1995, **4**, 2411-2423.

60 Z. Zhang and A. G. Marshall, *J. Am. Soc. Mass. Spectrom.*, 1998, **9**, 225-233.

61 A. A. Klammer and M. J. MacCoss, *J. Proteom. Res.*, 2006, **5**, 695-700.

## Figure legends

**Figure 1.** Chemical reaction catalyzed by HTP.

**Figure 2.** SDS-PAGE (12%) analyses for the two chromatographic steps of purification of recombinant HTP. Lane 1, Molecular Weight Page Ruler Marker (Fermentas); lane 2, crude extract; lane 3, Q-Sepharose Fast Flow anion exchange elution; lane 4, HiLoad Phenyl Sepharose High Performance hydrophobic interaction elution.

**Figure 3.** Determination of HTP molecular mass by mass spectrometry analysis. (A) ESI-FTMS spectra with HTP charge state distribution from 29+ to 65+. (B) Deconvoluted spectra of HTP resulted in a peak corresponding to a molecular mass value of 48,855 Da.

**Figure 4.** Determination of apparent steady-state kinetic constants. (A) Hyperbolic dependence of specific activity of recombinant HTP on increasing  $P_i$  concentrations at fixed concentration of dThd (400  $\mu$ M). (B) Dependence of HTP specific activity on increasing dThd concentrations at fixed concentration of  $P_i$  (2 mM), showing dThd substrate inhibition.

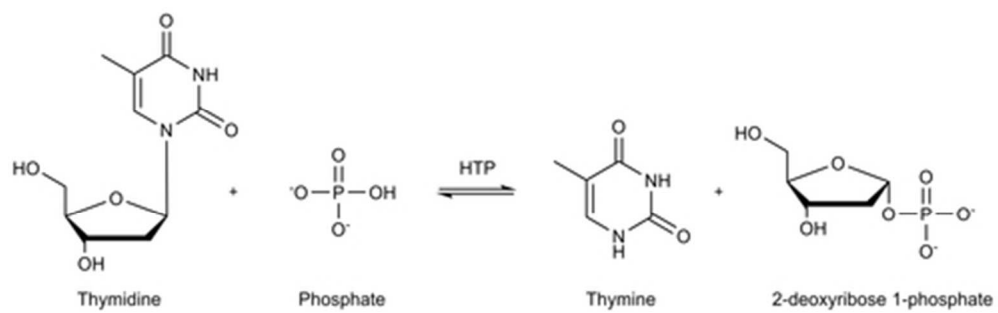
**Fig. 5.** Intersecting initial velocity patterns for HTP with either dThd (A) or  $P_i$  (B) as the variable substrate. Each curve represents fixed-varying levels of the co-substrate.

**Fig. 6.** Isothermal titration calorimetric (ITC) curves for binding of ligands to HTP. (A) Titration of dThd at a final concentration of 165  $\mu$ M. (B) Titration of  $P_i$  at a final

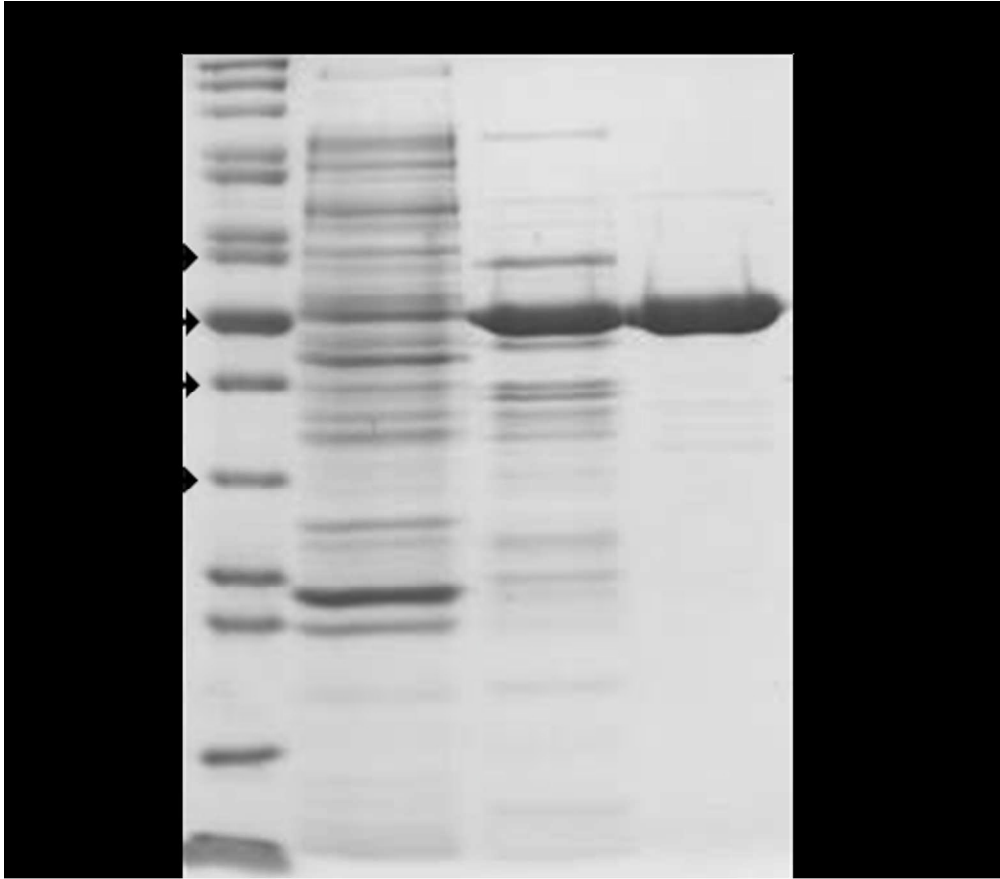
concentration of 497  $\mu\text{M}$ . (C) Titration of thymine at a final concentration of 828  $\mu\text{M}$ .  
(D) Titration of 2dR1P at a final concentration of 580  $\mu\text{M}$ .

**Fig. 7.** Proposed kinetic mechanism for HTP.

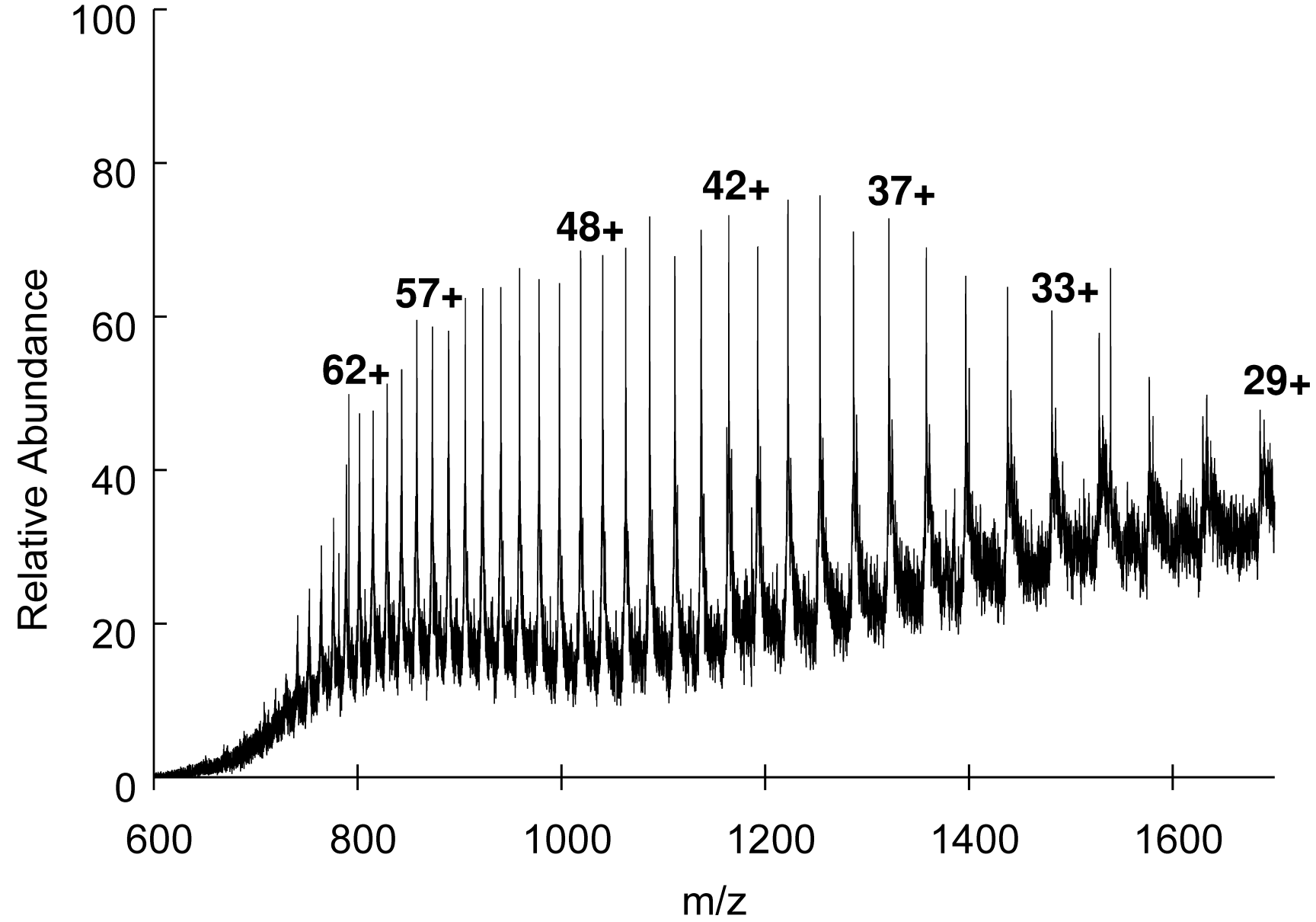
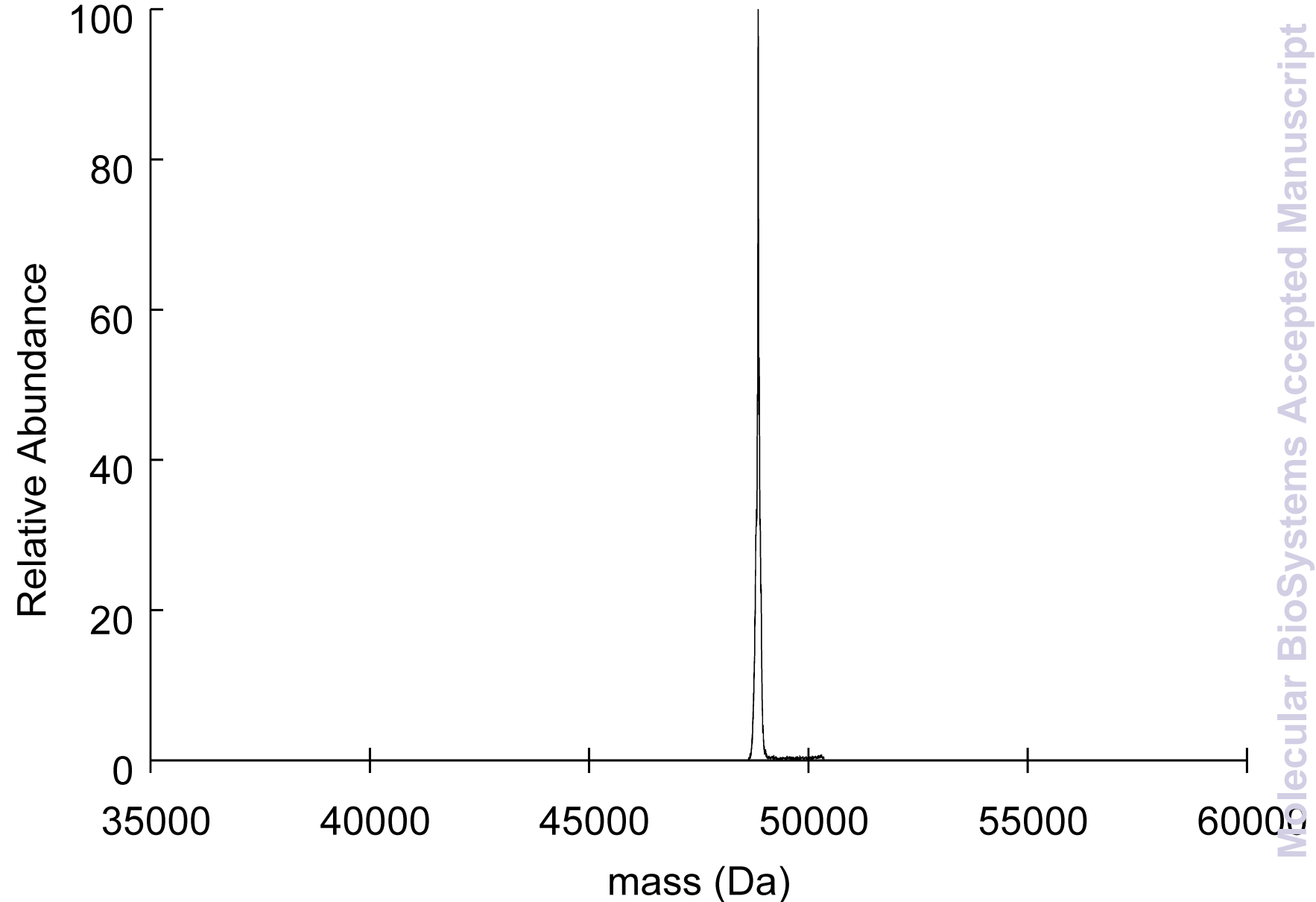
**Fig. 8.** Dependence of kinetic parameters on pH. (A)  $\log k_{\text{cat}}$ ; (B)  $\log k_{\text{cat}}/K_{\text{dThd}}$ ; (C)  $\log k_{\text{cat}}/K_{\text{Pi}}$ .

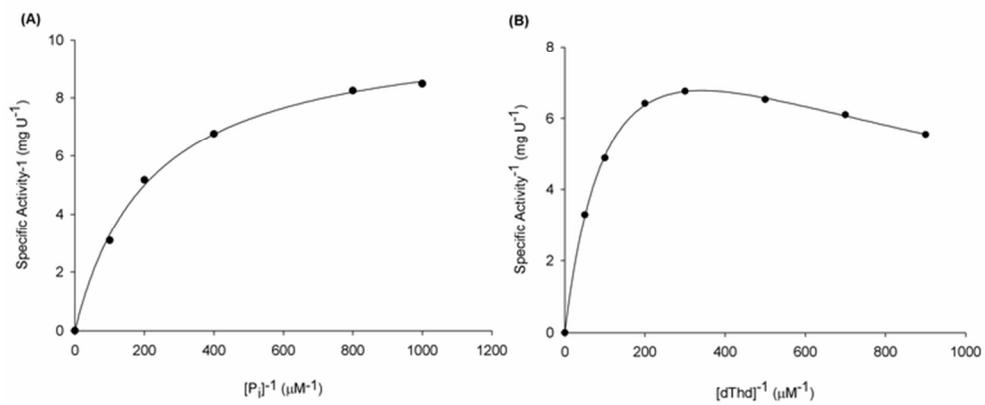


41x13mm (300 x 300 DPI)

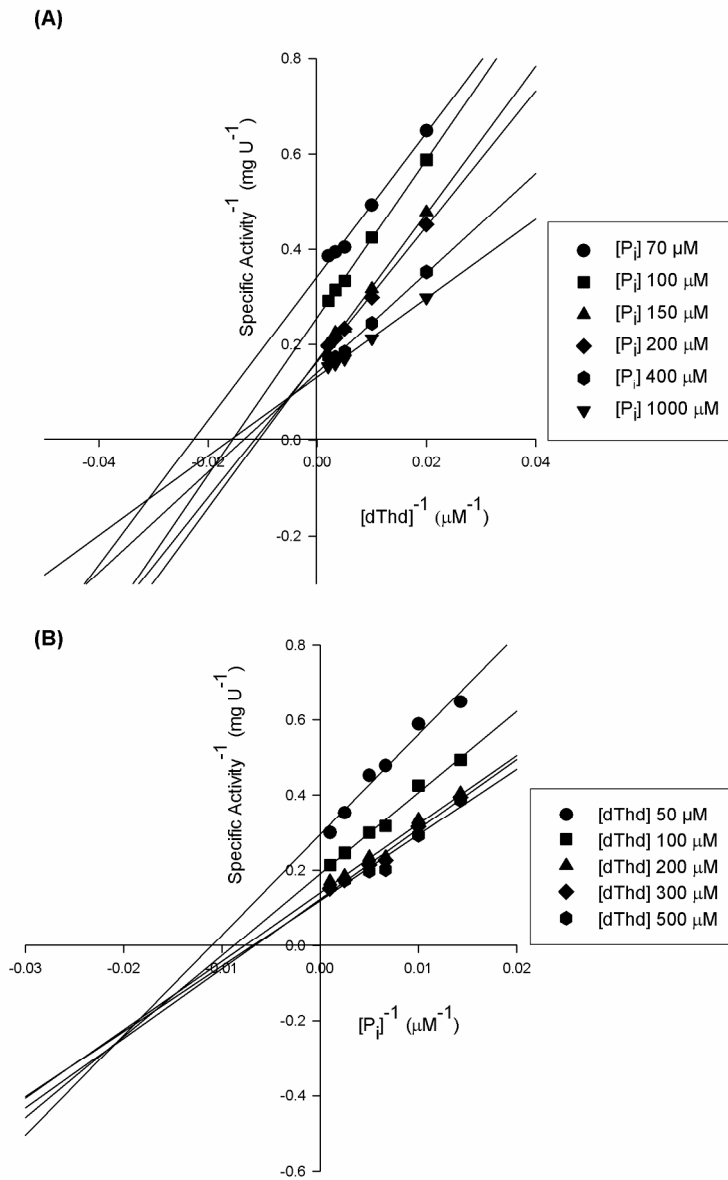


81x71mm (300 x 300 DPI)

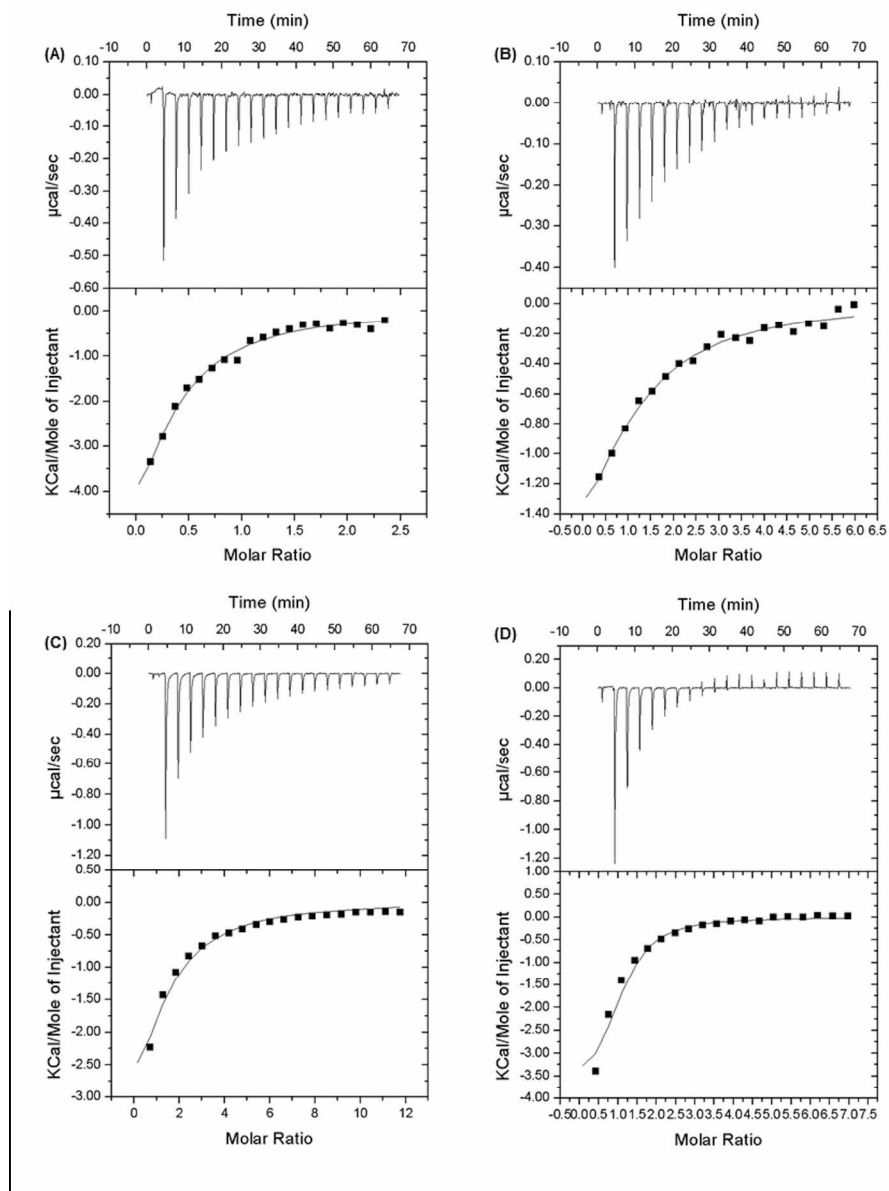
**(A)****(B)**



66x29mm (300 x 300 DPI)



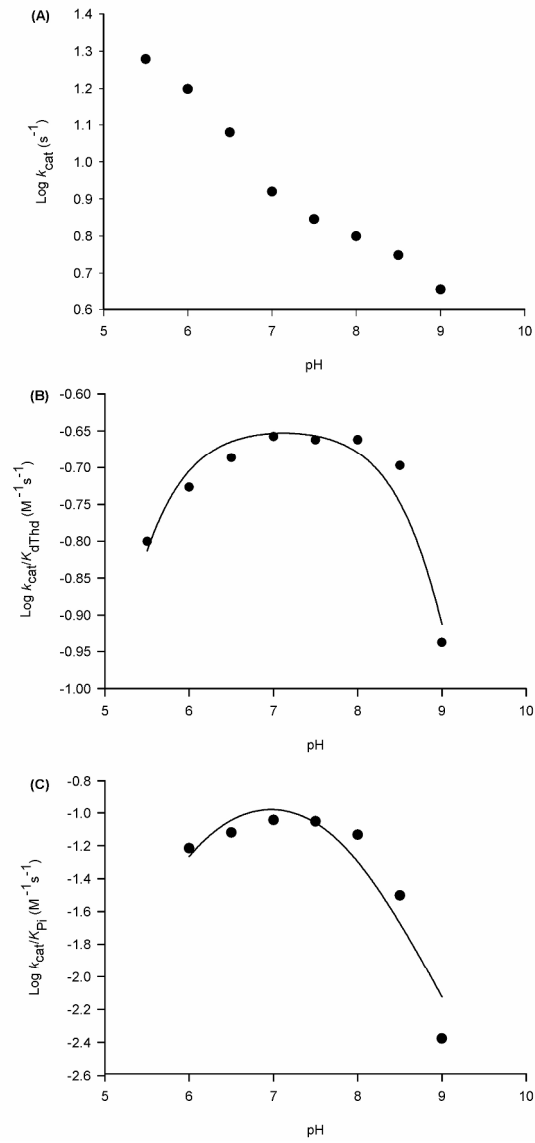
331x459mm (150 x 150 DPI)



170x220mm (300 x 300 DPI)



20x3mm (300 x 300 DPI)



331x663mm (150 x 150 DPI)